Revisiting the phase transitions of the Dicke model

Pragna Das and Auditya Sharma
Indian Institute of Science Education and Research, Bhopal 462066, India

(Received 24 September 2021; accepted 7 March 2022; published 30 March 2022)

The Dicke model exhibits a variety of phase transitions. The quantum phase transition from the normal phase to the super-radiant phase is marked by a dramatic change in the scaling of the participation ratio. We find that the ground state in the super-radiant phase exhibits multifractality manifest in the participation ratio scaling as the square root of the full Hilbert-space dimension. The thermal phase transition temperature, for which an exact analytical expression may be obtained using the partition function, is strikingly captured by the mutual information between two spins. In the excited-state quantum phase transition within the super-radiant phase, there are two cutoff energies; the central energy bands between the lower and upper cutoff energies show distinctly different behaviors. While the level statistics of the central band is Wigner-Dyson, the lower and upper bands show mixed behavior that is closer to Poisson than Wigner-Dyson. This finding is corroborated with the aid of several *eigenvector* properties: von Neumann entanglement entropy between spins and bosons, the mean photon number, concurrence between two spins, and participation ratio.

DOI: 10.1103/PhysRevA.105.033716

I. INTRODUCTION

The Dicke model, which incorporates the interactions of an ensemble of N two-level atoms via dipole coupling with a single bosonic mode [1–7], has its origin in quantum optics, but has found application in a wide range of fields from quantum chaos to quantum entanglement [8–22] to scrambling and thermalization [23]. Besides possessing an intimate connection to experiments [24–26], the Dicke model is a testbed for a variety of phase transitions [27]. Although a lot is known about these different transitions, the literature presents a rather scattered treatment of them [27–34]. In this paper, we revisit the three different kinds of phase transitions in the Dicke model, with the aid of a variety of localization and entanglement measures.

The nature of the ground state of the Dicke model is dramatically different depending on the magnitude of the coupling between the atoms and the field. While for small coupling, in the normal phase (NP), the average photon number in the ground state is close to zero, when the coupling is greater than a critical value, in the super-radiant phase (SP), the ground-state mean photon number scales linearly with the number of atoms [27–30]. Entanglement properties [19–21] offer clear signatures of this quantum phase transition [35–40] (QPT). Furthermore, a study of level statistics suggests that the system in fact also undergoes a transition from quasi-integrable to quantum chaotic [20] at the QPT. However, a later study by Chávez-Carlos *et al.* [41] argues that there is no direct relationship between the QPT and the onset chaos, and the simultaneous occurrence of these two is a consequence of the special choice of system parameters. In this paper, with the aid of a careful study of the participation ratio (PR) [42] of the ground state, we show how the normal to super-radiant phase transition is really a localization-to-multifractal transition. We find that in the super-radiant phase the ground-state participation ratio scales as the square root of the full Hilbert-space dimension.

The Dicke model also exhibits a thermal phase transition (TPT) which was realized many decades ago [31,32]. When the coupling is greater than the critical coupling, as the temperature is increased, we see a transition back from the super-radiant to the normal phase [33]. Generalizing the approach of Wang and Hieo [32], we are able to write down an exact analytical expression for the transition temperature, as has also been obtained by other authors [33,43]. We begin by writing down the partition function as a double integral, which may then be evaluated, in the thermodynamic limit, using the method of steepest descent. The transition temperature is identified to be the point at which the method of steepest descent breaks down. Furthermore, just like entanglement in the ground state marks the quantum phase transition, we show how the mutual information (MI) between atoms offers a striking signature at the thermal phase transition.

The Dicke model also exhibits an excited-state quantum phase transition (ESQPT), a term that is used to denote criticality in the excited states of a quantum system [33,34,44–47]. The ESQPT, which is a generalization of the QPT, and is characterized by abrupt variations of the energy and other excited-state properties at a sharp critical value of the energy [48], must be viewed in the backdrop of the tremendous recent interest in the properties of excited states [44,49–55] of quantum systems. In the present paper, we uncover how the ESQPT of the Dicke model affects not only energy levels below a certain lower cutoff but also the top-lying energy levels above a second *upper* cutoff, a feature that has been recognized in the literature [33,56–59] but is still not universally accepted [23,53]. We show how an energy-resolved study of eigenvalue

properties like level statistics [60] and the consecutive level spacing ratio [61] helps to clearly separate the nature of the central band from the top and bottom bands, in the superradiant phase. Strikingly, in contrast to prior studies, we are able to identify these features with the aid of several *eigenstate* properties: von Neumann entanglement entropy (VNEE), the mean photon number, concurrence, and PR.

II. HAMILTONIAN AND OBSERVABLES

The Hamiltonian of the Dicke model is

$$\mathcal{H} = \omega a^\dagger a + \omega_0 J_z + \frac{g}{\sqrt{2j}}(a + a^\dagger)(J_+ + J_-) \tag{1}$$

where a and $a^\dagger$ are bosonic operators, ω is the single-mode frequency of the bosonic field while ω_0 is the level splitting of the atoms, and g is the coupling strength of the light-matter interaction. We work in units where $\hbar = 1$ and $\omega = \omega_0 = 1$, thus the bosonic commutation relation is $[a, a^\dagger] = 1$. The angular momentum operators $J_{\pm,z} = \sum_{i=1}^{2j} \frac{1}{2}\sigma_{\pm,z}^{(i)}$ correspond to a pseudospin with length j, composed of $N = 2j$ spin-$\frac{1}{2}$ atoms described by Pauli matrices $\sigma_{\pm,z}^{(i)}$ acting on site i and satisfy the commutation relations $[J_z, J_\pm] = \pm J_\pm$, $[J_+, J_-] = 2J_z$. The basis of the full Hilbert space of the system is $\{|n\rangle \otimes |j, m\rangle\}$ where $|n\rangle$ are the bosonic basis states satisfying $a^\dagger a|n\rangle = n|n\rangle$ and $|j, m\rangle$ are the Dicke states satisfying $J_\pm|j, m\rangle = \sqrt{j(j+1) - m(m \pm 1)}|j, m \pm 1\rangle$, $J_z|j, m\rangle = m|j, m\rangle$. In our paper, we take N to be even, and consider the symmetric subspace which fixes $j = \frac{N}{2}$, and thus m takes the $(N + 1)$ values $(-\frac{N}{2}, \ldots, 0, \ldots, \frac{N}{2})$. We also truncate the bosonic mode to take the values $n = 0, 1, \ldots, n_{\max}$. Thus the dimension of the Hilbert space is given by $N_D = (N + 1)(n_{\max} + 1)$. In the thermodynamic limit the system shows a second-order quantum phase transition from the NP to the SP at $g = \frac{\sqrt{\omega\omega_0}}{2}$ $(= g_c)$ [20]. In the units that we work in throughout this paper, the critical coupling strength is $g_c = 0.5$.

Next we briefly describe the observables that will be studied ahead.

A. Inverse participation ratio and multifractal dimension

The inverse participation ratio (IPR) [62] of an eigenstate $|\psi\rangle = \sum_j^{N_D} \psi_j|j\rangle$ [where N_D is the Hilbert-space dimension and we continue to work in the $\{|n\rangle \otimes |j, m\rangle\}$ basis, as mentioned right after the system Hamiltonian in Eq. (1)] is defined as

$$P^{-1} = \sum_{j=1}^{N_D} |\psi_j|^4. \tag{2}$$

It is useful to quantify the degree of delocalization of the eigenstate. A finer understanding of the localization properties may be obtained by studying the multifractal dimension [63,64]:

$$D_q = \frac{S_q}{\ln(N_D)} \tag{3}$$

where $S_q = \frac{1}{1-q} \ln\left(\sum_{j=1}^{N_D} |\psi_j|^{2q}\right)$ is known as the q-dependent participation entropy. In the Shannon limit $(q = 1)$, $S_1 = \sum_j |\psi_j|^2 \ln(|\psi_j|^2)$, while $q = 2$ is related to the usual IPR with $S_2 = -\ln(P^{-1})$. S_∞ is determined by the maximum value of the densities $p_{\max} = \max_j |\psi_j|^2$ and $D_\infty = -\frac{\ln(p_{\max})}{\ln(N_D)}$. For a perfectly delocalized state $S_q = \ln(N_D)$ (when N_D is large) and hence $D_q = 1$ for all q. On the other hand for a localized state $S_q = \text{const}$ and $D_q = 0$. In an intermediate situation, wave functions are extended but nonergodic with $S_q = D_q \ln(N_D)$ where $0 < D_q < 1$ and the state is multifractal.

B. Q measure, von Neumann entanglement entropy, concurrence, and mutual information

The so-called Meyer and Wallach Q measure [52,65–67], defined as

$$Q = 2\left[1 - \text{Tr}\left(\rho_1^2\right)\right], \tag{4}$$

is a measure of how mixed a single spin is, and has proven to be a useful marker of a quantum phase transition.

The standard measure of entanglement [68] when the overall state is pure is the VNEE [19]. For our model, it is convenient to study the VNEE between spins and bosons given by

$$S = -\text{Tr}(\rho_{\text{boson}} \log_2 \rho_{\text{boson}}), \tag{5}$$

where $\rho_{\text{boson}} = \text{Tr}_{\text{atom}}\rho$ is the reduced density matrix of the bosonic part.

The concurrence [69–72] between (any) two atoms is given by

$$C = \max\{0, \lambda_1 - \lambda_2 - \lambda_3 - \lambda_4\}, \tag{6}$$

where λ_i are the square roots of the eigenvalues of the matrix product, $\tilde{\rho}_{12} = \rho_{12}(\sigma_{1y} \otimes \sigma_{2y})\rho_{12}^\star(\sigma_{1y} \otimes \sigma_{2y})$, in descending order $(\lambda_1 > \lambda_2 > \lambda_3 > \lambda_4)$. Here $\rho_{12}^\star$ denotes complex conjugation of ρ_{12}, and σ_{iy} are Pauli matrices for two-level systems. Concurrence is a good measure of entanglement in both pure and mixed states. Therefore, for the Dicke model, it is useful to study concurrence between any two spins in the eigenstates of the model, in time-evolved states of quench dynamics and also thermal mixed states.

When the overall state is mixed, the MI between two subsystems A and B is a useful measure of the total correlations between A and B. Specifically, we define the mutual information I_{AB} [73–76] as

$$I_{AB} = S_A + S_B - S_{AB}, \tag{7}$$

where $S_{A,B} = -\text{Tr}[\rho_{A,B} \ln(\rho_{A,B})]$ and $S_{AB} = -\text{Tr}[\rho_{AB} \ln(\rho_{AB})]$ are the corresponding von Neumann entropies of the states ρ_A, ρ_B, and ρ_{AB} respectively. For the Dicke model, we will see that it is particularly convenient to study the mutual information between two spins, which we denote by I_{12}.

We emphasize that to calculate the Meyer and Wallach Q measure and the mutual information we have written the system Hamiltonian in the spin product space basis. The size of the Hamiltonian matrix is $N_D \times N_D$ where $N_D = (n_{\max} + 1) \times 2^N$.

III. QUANTUM PHASE TRANSITION

A. Statics

In Fig. 1(a) we exhibit the Q measure for the ground state of the system as a function of coupling parameter g.

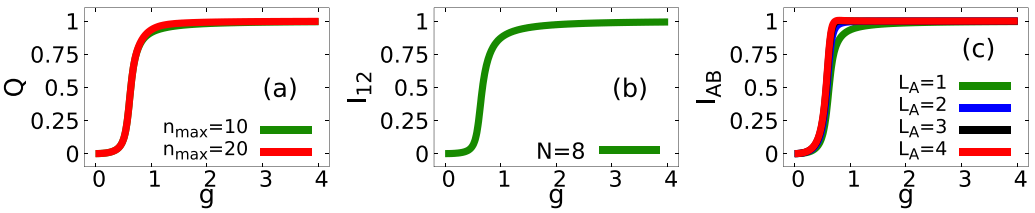

FIG. 1. (a) The Meyer and Wallach Q measure of the ground state as a function of coupling, g. Number of spins $N = 8$. (b) Mutual information between two spins. (c) Mutual information between two spin subsectors. Here we divide the spins into two subsectors with spin number L_A and L_B. The total number of spins can be broken into $N = 8 = L_A + L_B = 1 + 7 = 2 + 6 = 3 + 5 = 4 + 4$. For panels (b) and (c) $n_{\max} = 10$.

Here ρ_1 is the single atomic reduced density matrix and it can be calculated by tracing out the bosonic part first and then over the $N - 1$ atoms. Q is close to zero for $g < g_c$ (NP) and close to 1 for $g > g_c$ (SP) with a transition near the critical point. It goes to zero when $\mathrm{Tr}(\rho_1^2) \approx 1$, i.e., in the NP the single atom reduced density matrix behaves like a pure state having the two eigenvalues close to 1 and 0. On the other hand $Q \approx 1$, when $\mathrm{Tr}(\rho_1^2) \approx 0.5 < 1$, hence ρ_1 is nearly a maximally mixed state in the SP.

To calculate the mutual information between two groups of spins, we first take a partial trace of the total density matrix over the bosonic part followed by a partial trace over one group of the spins. Figure 1(b) shows the mutual information between two spins of the Dicke model. I_{12} is close to zero in the NP and close to 1 in the SP with a transition near the critical point. Hence we can say that the total correlation between two spins is zero in the NP whereas in the SP the correlation is maximum. Thus I_{12} significantly depends on the spin boson coupling g. Figure 1(c) shows the mutual information between two groups of spins A and B, in which group A contains L_A spins while group B contains the remaining $L_B = N - L_A$ spins. Because of the symmetry in the coupling it does not matter which L_A spins are considered. We see that this quantity too shows similar behavior as I_{12}. From Fig. 1(a) we conclude that in the NP each spin is separately in a pure state, so there are no quantum correlations at all. On the other hand in the SP, we see that all the correlations are very high. Specifically, the correlations between two spin groups containing L_A and L_B spins are all high no matter what value L_A takes.

Figure 2(a) shows an exact diagonalization study of the IPR of the ground state as g is varied; we observe that it is close to 1 in the NP and close to zero in the SP. Thus we see that the ground state is localized in the NP whereas it is extended in nature in the SP. The inset of Fig. 2(a) illustrates the participation ratio PR (which is the inverse of the IPR) as a function of the coupling g and it shows a phase transition from the NP where it takes values close to zero to the SP with a sharp transition to a nonzero value at the critical coupling. We plot the PR for different atom number N and notice that in the SP the value of PR increases with N.

In Fig. 2(b) we show D_1, D_2, and D_∞ for the ground state as a function of the coupling parameter g. In the NP $D_q \approx 0$ and hence we can say that the ground state is localized in the NP. Contrastingly in the SP, $0 < D_q < 1$ with $D_1 > D_2 > D_\infty$ ($D_1 \approx 0.58$, $D_2 \approx 0.55$, $D_\infty \approx 0.47$), with a sharp transition at the critical point. In the inset of Fig. 2(b) we show that at $g = 4.0$ the PR goes as the square root of the Hilbert-space dimension. Hence we find that the SP is neither perfectly delocalized nor localized, and in fact displays multifractal character [63]. Given the intense current interest in multifractal states [77–79], this discovery in a familiar model is an exciting finding.

B. Dynamics

We next describe how the quantum phase transition in the Dicke model is usefully studied with a quenching protocol [80]. In a quantum quench, we prepare a closed system in an eigenstate of one Hamiltonian $\mathcal{H}_0$ and then have the system evolve dynamically in time under a different Hamiltonian

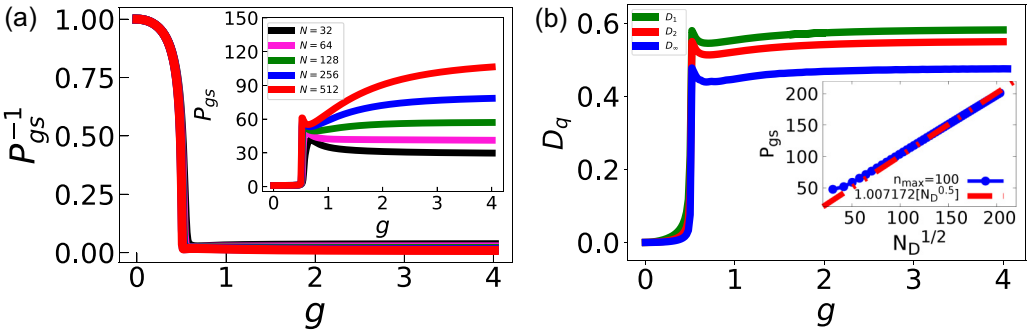

FIG. 2. (a) The IPR of the ground state as a function of coupling g. The inset shows a similar plot for the PR. (b) Multifractal dimension D_q ($q = 1, 2, \infty$) of the ground state as a function of g. The inset shows the scaling of PR with atom number N for the ground state at $g = 4.0$. In all the figures, we set $N = 512$, $n_{\max} = 32$.

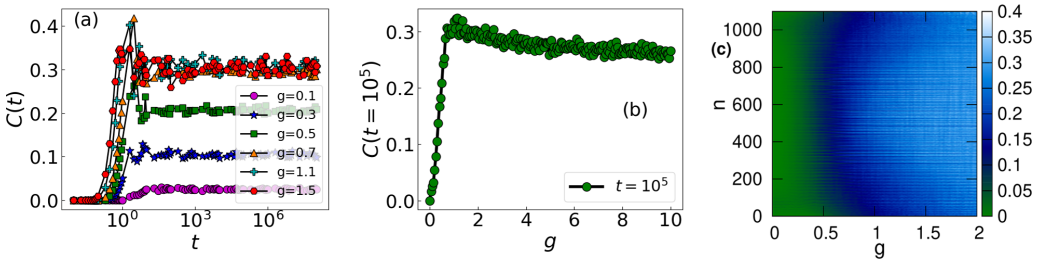

FIG. 3. (a) Concurrence between two atoms as a function of time $C(t)$ for different coupling strengths. (b) Saturation value of concurrence at time $t = 10^5$ as a function of coupling strength g. The parameters for panels (a) and (b) are $N = 128$, $n_{\max} = 32$. (c) Quench dynamics of concurrence C, at time $t = 10^6$. $C(t = 10^6)$ as a function of coupling parameter g and n (index for the eigenstates of the decoupled Hamiltonian $\mathcal{H}_0$ accordingly). Green color denotes NP and blue color denotes SP. Parameters are $N = 128$, $n_{\max} = 16$.

$\mathcal{H} = \mathcal{H}_0 + \mathcal{H}_1$. For our problem, we take $\mathcal{H}_0$ to be the Dicke model with $g = 0$, and the middle excited state of $\mathcal{H}_0$ as our initial state. The value of g is then suddenly changed to some other nonzero value of g, and the resulting dynamics of the system is studied. The concurrence (between any two atoms) as a function of time $C(t)$ is shown for a range of values of g in Fig. 3(a). In general, $C(t)$ starting from zero remains close to zero up to $t \approx 0.1$, after which it increases up to $t \approx 10$. With further increase of time, it tends to saturate to a constant with some fluctuations. This saturating value of $C(t)$ depends on g, and carries information of the quantum phase transition. For $g = 0.1$ (pink circles) the saturation value of concurrence is close to zero, but with increasing g, the saturation value increases gradually until a certain critical g_c. Beyond g_c (green squares) we begin to see a saturating tendency of the saturation value itself with some fluctuations [see Fig. 3(a)]. This feature is made clearer by a plot of the saturation value of the concurrence at some late time, say $t = 10^5$ as a function of the coupling parameter g as shown in Fig. 3(b). We observe that in the NP the saturation value is increasing with g, but after crossing the critical point g_c in the SP it is almost independent of g, i.e., the value is constant with some fluctuations. Thus we see that the dynamics too shows signatures of the quantum phase transition. In Fig. 3(c) we study the dynamics starting from each of the eigenstates of the decoupled Hamiltonian, $\mathcal{H}_0 = \omega a^\dagger a + \omega_0 J_z$, and evolving with the unitary time evolution operator $U = e^{-i\mathcal{H}t}$ where $\mathcal{H}$ is the system Hamiltonian. For a particular coupling strength g, U is fixed but the initial states are changing and hence $|\psi_i(t)\rangle = U|\psi_i(0)\rangle = U|i\rangle$, where $\{|i\rangle\}$ are the eigenstates of $\mathcal{H}_0$. We plot the concurrence (between any pair of atoms) with respect to the time evolved. We see that Fig. 3(c) shows that the dynamics is sensitive to the quantum phase transition no matter which eigenstate we start from.

IV. THERMAL PHASE TRANSITION

To compute the partition function [43,81,82] [$Z = \mathrm{Tr}(e^{-\frac{\mathcal{H}}{k_B T}})$] of the Dicke Hamiltonian it is useful to first write it in units of ω as

$$\tilde{\mathcal{H}} = \frac{\mathcal{H}}{\omega} = a^\dagger a + \sum_{j=1}^{N} \frac{\epsilon}{2}\sigma_j^z + \frac{\lambda}{\sqrt{N}} \sum_{j=1}^{N} (a + a^\dagger)\sigma^x \quad (8)$$

where $\epsilon = \frac{\omega_0}{\omega}$ and $\lambda = \frac{g}{\omega}$. Following the method of Wang and Hieo [32] (who studied the Dicke model within the rotating wave approximation), the partition function can be computed as

$$Z(N,T) = \sum_{s_1,\ldots,s_N=\pm 1} \int \frac{d^2\alpha}{\pi} \langle s_1,\ldots,s_N| \times \langle\alpha|e^{-\beta\tilde{\mathcal{H}}}|\alpha\rangle|s_1,\ldots,s_N\rangle. \quad (9)$$

The expectation value of the Hamiltonian with respect to the bosonic modes is obtained in a straightforward manner:

$$\langle\alpha|\tilde{\mathcal{H}}|\alpha\rangle = \alpha^*\alpha + \sum_{j=1}^{N}\left[\frac{\epsilon}{2}\sigma_j^z + \frac{\lambda}{\sqrt{N}}(\alpha + \alpha^*)\sigma_j^x\right]. \quad (10)$$

Defining

$$h_j = \frac{\epsilon}{2}\sigma_j^z + \frac{\lambda}{\sqrt{N}}(\alpha + \alpha^*)\sigma_j^x \quad (11)$$

the expectation value with respect to the spins becomes a product of single-spin expectation values:

$$\langle s_1,\ldots,s_N|\langle\alpha|e^{-\beta\tilde{\mathcal{H}}}|\alpha\rangle|s_1,\ldots,s_N\rangle = e^{-\beta|\alpha|^2}\Pi_{j=1}^{N}\langle s_j|e^{-\beta h_j}|s_j\rangle. \quad (12)$$

Thus the computation of the partition function reduces to the evaluation of a double integral:

$$Z(N,T) = \int \frac{d^2\alpha}{\pi} e^{-\beta|\alpha|^2}\left(2\cosh\left\{\frac{\beta\epsilon}{2}\left[1 + \frac{16\lambda^2\alpha^2}{\epsilon^2 N}\right]^{1/2}\right\}\right)^N \quad (13)$$

which in the thermodynamic limit ($N \to \infty$), may be carried out with the aid of the method of steepest descent, within the super-radiant phase. Tracking the point at which the method breaks down (see the Appendix), we obtain an exact expression for the transition temperature:

$$T_c = \frac{1}{\beta_c} = \left(\frac{\omega_0}{2\omega}\right)\frac{1}{\tanh^{-1}\left(\frac{\omega\omega_0}{4g^2}\right)}. \quad (14)$$

The critical temperature expression is meaningful only when $g > g_c$. When $g < g_c$, the system is in the normal phase at all temperatures. When $g > g_c$, it is only above the critical temperature that the system is in the normal phase, while for $T < T_c$ the system is in the super-radiant phase.

A study of the mutual information between (any) two spins in the thermal density matrix proves to be profitable. In Fig. 4(a) we show I_{12} as a function of temperature at $g = 1$

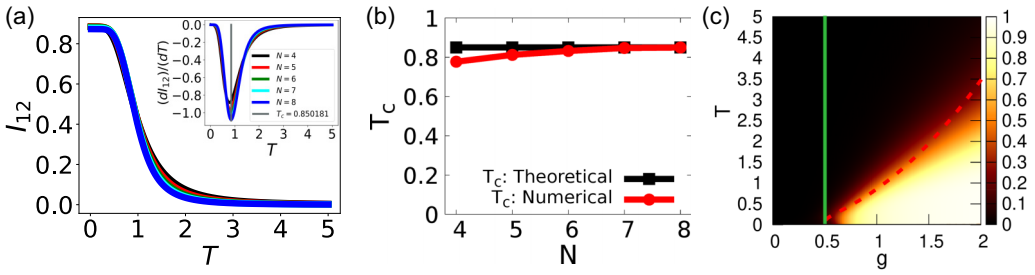

FIG. 4. (a) MI of two spins as a function of temperature at $g = 1.0$, with the inset showing the numerical derivative of MI with respect to temperature $\frac{dI_{12}}{dT}$. (b) The red line with solid circles denotes the critical temperature as a function of atom number N, while the black line with a solid square is the theoretical value ($T_c = 0.850\,181$) for $g = 1.0$. (c) Mutual information of two spins as a function of coupling g and temperature T. The parameters are $N = 6$, $n_{\max} = 10$. The dark region corresponds to the NP, and the bright region corresponds to the SP. The solid line corresponds to g_c and the dashed line denotes the critical temperature theoretically calculated in Eq. (A11). In all the plots $\omega = \omega_0 = 1$.

($g > g_c$). At low temperatures in the SP, I_{12} takes a value close to unity while at high temperatures in the NP, I_{12} drops to a value close to zero, with a dramatic drop happening at a temperature close to the transition temperature. For a finer understanding of the variation of the mutual information across the transition, we study in the inset of Fig. 4(a) the first-order temperature derivative $\frac{dI_{12}}{dT}$, for different atom numbers. We observe that the temperature at which the derivative takes the minimum value is consistent with the transition temperature T_c, denoted by the vertical line. Figure 4(b) confirms that as the number of atoms is increased the temperature at the minimum does indeed approach the theoretically obtained critical temperature. From the surface plot of the MI as a function of g and T in Fig. 4(c), it is clear that for $g < g_c$ there is no phase transition, but for $g > g_c$ there exists a critical temperature T_c at which the system changes from the super-radiant phase ($T < T_c$) to the normal phase ($T > T_c$).

To calculate the mutual information between two spins we have to take the partial trace of the total thermal density matrix $\rho_{\text{th}} = e^{-\frac{\mathcal{H}}{k_B T}}$ first over the bosonic subspace and next over the $(N-2)$ atoms. Hence in this case we have to use the product space for the atoms, and are thus forced to diagonalize matrices of size $(n_{\max}+1) \times 2^N$. So we end up working with rather modest system sizes with atom number $N = 6$ and $n_{\max} = 10$. However, although the dimension is low here still our numerics seems to broadly agree with the transition given by the analytical result. While it is widely known that entanglement in the ground state signals the QPT, our paper shows that despite also including classical correlations the mutual information between atoms offers a striking signature at the thermal phase transition.

V. EXCITED-STATE QUANTUM PHASE TRANSITION

The Dicke model exhibits an excited-state quantum phase transition in the super-radiant phase. When $g > g_c$, it has been reported [23,53] that the eigenvalues above a cutoff energy E_c behave in a distinctly different manner in comparison with the eigenvalues below the cutoff. We find that in fact there is not just a lower cutoff, but also an upper cutoff as has been recognized in the literature [33,56–59], although it is not widely appreciated [23,53]. Our data show that we must study separately the eigenvalues drawn from a central band composed of energy levels between a lower and upper cutoff. The lower and upper energy bands show different behaviors. While eigenvalue properties like level statistics and gap ratio provide supporting evidence, we highlight how *eigenstate properties* offer a striking demonstration of this picture.

A. Eigenvalue properties

The onset of ergodic behavior is typically diagnosed by inspection of the level spacing distribution [60]. Let $\{E_n\}$ denote the energy levels of the DM in ascending order. Under the assumption that the density of states (DOS) equals unity, the distribution $P(s)$ of the level spacings $s_n = E_{n+1} - E_n$ is given by the Poisson distribution $P(s) = \exp(-s)$ in the normal phase [83]. On the other hand, in the super-radiant phase, the level spacings adhere to the Wigner-Dyson distribution $P(s) = \frac{\pi}{2} s \exp[-(\pi/4)s^2]$ [84]. To study the level statistics we consider two g values: $g = 0.2 < g_c$ and $g = 4.0 > g_c$. For $g < g_c$ we see that the energy spacings are consistent with the Poisson distribution. For $g > g_c$ we study the level statistics separately in three bands as shown in Fig. 5. While the energy spacing distribution for levels that lie between the lower and upper cutoff energies is like the Wigner-Dyson distribution, the level spacing distributions of the upper and lower energy bands show mixed behavior, although the distribution looks more Poissonian than Wigner-Dyson. Evidently, there is a striking absence of level repulsion in these bands, in stark contrast to the levels in the central band. While the presence of the lower cutoff is well known [23,53], our data clearly show an upper cutoff as well [33,56–59].

The above picture with respect to the energy levels is further strengthened by a study of the ratio of consecutive level spacings, which has now become a standard measure [61,85]. Let s_n denote level spacing between two consecutive energies E_{n+1} and E_n. The average spacing ratio $\langle r \rangle$ is defined as the average over n of the ratio of consecutive level spacings:

$$r_n = \frac{\min(s_{n-1},\ s_n)}{\max(s_{n-1},\ s_n)}. \tag{15}$$

From random matrix theory it is known that [61] $\langle r \rangle$ takes a value $\langle r \rangle \approx 0.386$ for quasi-integrable Hamiltonians and $\langle r \rangle \approx 0.5307$ for Hamiltonians from the Gaussian orthogonal ensemble. $g < g_c$ $\langle r \rangle \approx 0.386$ and $g > g_c$ $\langle r \rangle \approx 0.5307$ for the

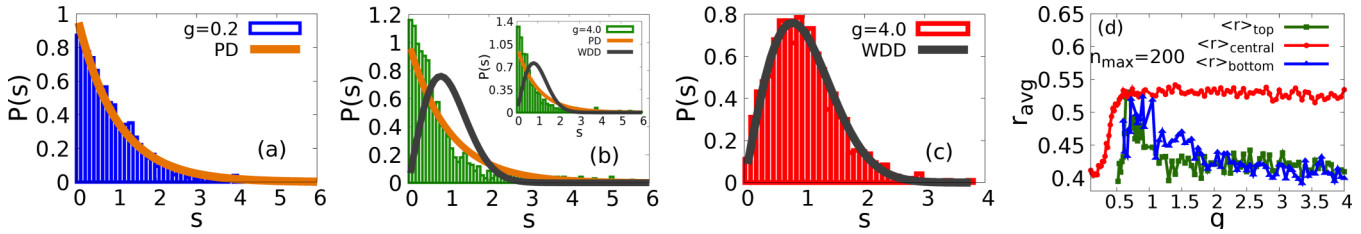

FIG. 5. Level statistics of the spectrum. (a) For $g < g_c$ the level spacing distribution is more like Poissonian. For $g > g_c$ there are three bands in the spectrum: below the lower cutoff energy (b), above the upper cutoff energy shown in the inset of panel (b), and the energies in between (c). The energy spacing distribution in between the lower and upper cutoff is more like Wigner-Dyson. However, in panel (b) the behaviors are not clear, as they show mixed behavior, although they are closer to Poissonian behavior. (d) r_{avg} value as a function of coupling, for the different energy bands. Blue triangles are used for energies below the lower cutoff, green squares are used for energies above the upper cutoff, and red solid circles are used for the middle band energies. Parameters are $n_{\text{max}} = 200$, $N = 60$.

central band. For the upper and the lower energy bands $\langle r \rangle$ lies in between 0.386 and 0.5307. However, we observe that as the coupling strength increases, and as the atomic number becomes large, they tend to resemble the Poissonian ensemble [see Fig. 5(d)].

B. Eigenvector properties

In Fig. 6(a) we show the VNEE [19] between spins and bosons for all the eigenstates of the Dicke model. We observe two cutoff energies: (i) lower cutoff energy (corresponding to the ground-state energy at $g = g_c$) and (ii) upper cutoff energy (corresponding to the maximum energy for $g = 0$). The value of VNEE is larger in the eigenstates of the central band in comparison with that of the top and bottom bands. Thus the eigenstates carry a clear signature of the two excited-state quantum phase transitions when $g > g_c$. In Fig. 6(b) we show a similar plot for the mean photon number [20] $\langle a^\dagger a \rangle$ which is scaled by the pseudospin length j of the system. It carries information pertaining to the bosonic part of the eigenstates. In the middle band the value of the mean photon number is comparatively lower than that of the other two bands. However, we observe that neither the VNEE between the atoms and the bosons nor the mean photon number is able to distinguish between the $g < g_c$ and $g > g_c$ regions of the middle band. A study of the entanglement between atoms provides useful further perspective.

In Fig. 6(c) we plot concurrence between two atoms for the whole spectrum as a function of g. We observe that in addition to showing a signature of the ESQPT in the super-radiant phase, concurrence is also able to distinguish the eigenstates of the middle band in the $g < g_c$ region and the $g > g_c$ region. In the NP, the concurrence value of the central states is comparatively smaller than that for the central states of the SP. Again the value of concurrence in the bottom and top bands of the super-radiant phase is a bit lower than that of the central band. Figure 6(d) shows the participation ratio of all the eigenstates as a function of coupling parameter g. We are able to identify the ESQPT, which divides the whole spectrum into three bands: top, bottom, and central. In the NP ($g < g_c$), the whole region shows a uniform comparatively small value of PR. On the other hand in the SP ($g > g_c$) while the central band exhibits a larger value of PR, the top and bottom bands show mixed behavior, although they resemble the NP more than the SP.

C. Finite-size scaling

Our data show that the lower and upper bands have qualitatively identical behavior and are distinctly different from the central band in the super-radiant phase. Specifically both the energy-resolved level statistics and level spacing ratio clearly indicate that the top band shows different statistics compared to the middle band. Hence one should separately study the level statistics in the different energy bands, separated by the lower cutoff energy and the E_*—we believe that an analysis that completely ignores the existence of E_* would be inaccurate. The literature has many studies [23,53] of level statistics that separately look at energy levels below E_c and above E_c, but with no mention of the upper cutoff. However, as our data show, the inclusion of the higher band energies in their level statistics study would make their Wigner-Dyson results noisy.

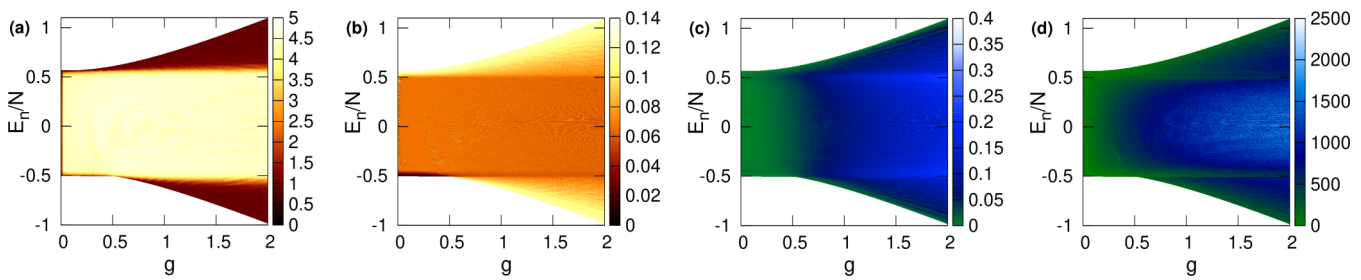

FIG. 6. (a) Von Neumann entanglement entropy between the atoms and the bosons as a function of coupling strength g and the energy density E_n/N (eigenenergy divided by the atom number N) of the DM. (b–d) Similar plots for mean photon number (b), concurrence between any two atoms (c), and participation ratio of the eigenstates (d). The parameters for all the four plots are $N = 512$, $n_{\text{max}} = 32$.

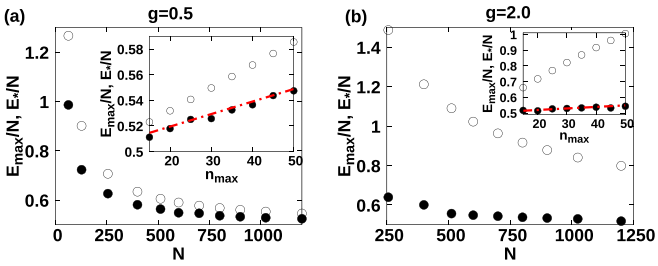

FIG. 7. Here $E_{\max}$ is the maximum energy of the system Hamiltonian and E_* is the energy where the von Neumann entanglement entropy between spin and boson suddenly drops [see Fig. 6(a)]. Energy density (energy scaled by the number of atoms), $E_{\max}/N$ (open circles) and E_*/N (solid black circles) as a function of atom number N, keeping $n_{\max} = 32$ fixed, (a) at $g = g_c = 0.5$ and (b) at $g = 2.0$. The insets show similar plots, but as a function of $n_{\max}$, keeping the atom number fixed at $N = 1024$. The red dash-dotted line in both the insets denotes the straight line $\frac{\omega}{N} n_{\max} + \frac{\omega_0}{2}$, which is seen to capture the E_*/N data for both the cases excellently.

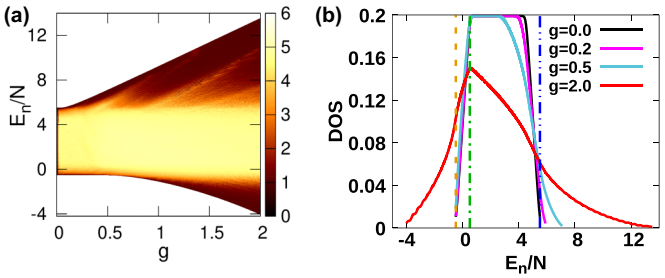

FIG. 8. (a) Similar plot of von Neumann entanglement entropy between spins and bosons, as Fig. 6(a) but for low atom number and high $n_{\max}$. (b) The density of states of the model at $g = 0.0$, 0.2, 0.5, and 2.0. Orange dashed line, $E/N = -0.5$; green dash-dotted line, $E/N = 0.5$; blue dash-double dotted line, $E/N = 5.5$. Here the atom number $N = 40$ and $n_{\max} = 200$.

The upper cutoff energy has been argued to be of a different nature in the literature [33,56–59]. One reason is the apparent extension of the upper cutoff even into the normal phase. In Fig. 7 we study the finite-size scaling of the upper cutoff point. Here $E_{\max}$ is the maximum energy of the system Hamiltonian (for finite N and $n_{\max}$) and E_* is the energy where the VNEE between spins and bosons suddenly drops [see Fig. 6(a)]. We plot these two energy densities ($E_{\max}/N$, E_*/N) as a function of the number of atoms N for two values of g: (i) at $g = g_c = 0.5$ and (ii) at $g = 2.0$ (in the super-radiant phase). In Fig. 7(b) for $g = 2.0$ (in the super-radiant phase) the gap between ($E_{\max}/N$, and E_*/N) remains robust even for large N. Thus, in the super-radiant phase, the upper cutoff appears as genuine as the lower cutoff.

On the other hand in the NP, from Fig. 7(a) one can notice that as N becomes large $E_{\max}/N$ and E_*/N almost overlap and tend to converge to the maximum energy density at $g = 0$. Hence one may be tempted to conclude that the upper cutoff point in the normal phase is a finite-size effect that disappears in the thermodynamic limit (when $N \to \infty$). However, a closer look at the finite-size scaling of the energy densities with $n_{\max}$ is revealing. Although the gap between $E_{\max}/N$ and E_*/N in the NP appears to vanish for very large N (while keeping $n_{\max}$ fixed), if we increase $n_{\max}$ (for a fixed atom number) the gap has an ever widening tendency albeit very slowly in the NP [inset of Fig. 7(a)]. Interestingly, the energy density at the upper cutoff (whether it is computed in the NP or the SP) agrees excellently with the equation

$$\frac{E_*}{N} = \frac{\omega}{N} n_{\max} + \frac{\omega_0}{2}. \tag{16}$$

The above equation corresponds to the maximum energy density for a system of N atoms and with the bosonic mode truncated at $n_{\max}$ in the $g = 0$ limit, where the highest energy is just given by all the spins being up. In the semiclassical approach of Brandes [56], the upper cutoff is argued to be exactly at $\frac{1}{2}\omega_0$, which would be consistent with our numerical data provided the limit $N \to \infty$ is taken before the $n_{\max} \to \infty$ limit. In Fig. 8(a) we show the VNEE (between spins and bosons) as in Fig. 6(a) but for low atom number ($N = 40$) and high $n_{\max}(= 200)$. We observe that in the super-radiant phase the VNEE has one abrupt change at the lower cutoff around $E_n/N = -0.5$, which is identified with the usual ES-QPT. However, there is also a sudden change in VNEE after $E_n/N = 5.5$ which we call the upper cutoff. This upper cutoff is not at 0.5 as in the semiclassical approach of Brandes [56]. If we go to the thermodynamic limit ($N \to \infty$) while keeping $n_{\max}$ finite, then our upper cutoff approaches 0.5.

In Fig. 8(b), we study the density of states of our finite-sized system using the formula

$$\mathrm{DOS}(E/N) = \frac{1}{N_D} \sum_{k=1}^{N_D} \delta(E/N - E_k/N), \tag{17}$$

for $g = 0.0$, 0.2, 0.5, and 2.0. For numerical calculation, one can replace the delta function by a Gaussian with small standard deviation. In this figure, the orange dashed line denotes the energy density $E/N = -0.5$ and the green dash-dotted line corresponds to $E/N = 0.5$. One can notice that between the densities -0.5 and 0.5 the DOS(E/N) behaves linearly with E/N, with positive slope. In the literature [33,56,57], the density of states is argued to be linear from -0.5 to 0.5, and to be a flat horizontal beyond 0.5. Our own numerical results suggest that the horizontal part is present only in the normal phase, and even in this case it begins to fall in linear fashion at a higher energy density. Moreover in the super-radiant phase, we see (look at the plot for $g = 2$) that beyond 0.5, there is another linear portion with a negative slope up to energy $E/N = 5.5$ (blue dashed double dotted line), after which the DOS behaves nonlinearly with E/N. The density of states in the central band (from -0.5 to 5.5) has two linear parts, one with a positive slope and the other with a negative slope. This is entirely consistent with the Wigner-Dyson statistics that the levels show for this region. A horizontal portion in the super-radiant phase would be inconsistent with Wigner-Dyson statistics, and thus we believe this feature could be an artifact of the semiclassical analysis of earlier studies [33,56,57]. The point at which the linear region (with negative slope) of the DOS ends is identified as our upper cutoff energy. The upper cutoff tends to 0.5, if the thermodynamic limit is taken while keeping $n_{\max}$ finite.

VI. SUMMARY

We study the phase transitions (QPT, TPT, ESQPT) of the Dicke model, with the aid of a number of measures of localization, entanglement, and mutual information. Different quantities are more suitable for the different kinds of phase transitions involved, and a comprehensive look at all of them helps us obtain an overall big-picture view of the Dicke model. The IPR for the ground state shows a sharp phase transition at g_c; while in the NP the ground state behaves like a localized state, the ground state in the SP is not localized. A careful study of the scaling of the PR (for the ground state in the SP) with the dimension N_D of the full Hilbert space reveals that the PR scales as $\sqrt{N_D}$, suggesting multifractal character. In the $g > g_c$ region there exists some critical temperature T_c, above which the SP disappears and the system goes into the NP whereas for $g < g_c$ the system remains in the NP for all temperatures. We obtain a closed-form expression for the transition temperature in the super-radiant phase, and numerically verify that the mutual information between two atoms provides a useful signature at the transition. Thus, at the temperature transition, the mutual information proves to be a worthy generalization of entanglement, which marks the ground-state QPT. We find that in the super-radiant phase the spectrum exhibits not only a lower cutoff but also an upper cutoff with the properties of the central band of energies distinctly different from the lower and upper bands. While the lower cutoff is an ESQPT that is well known in the literature, we argue that the upper cutoff too behaves like an ESQPT. Both these cutoffs are vividly captured by a number of eigenvector properties: VNEE, mean photon number, concurrence, and PR. For the VNEE and mean photon number the whole central band is uniform, with no distinction between $g < g_c$ and $g > g_c$ regions. We find that concurrence and PR reveal more structure. In addition to showing a signature of the ESQPT in the SP, these quantities are also able to distinguish the eigenstates of the central band between the $g < g_c$ region and $g > g_c$ region. Hence we are able to present various phase transitions in the DM in terms of several quantities that measure localization, multifractality, mutual information, and entanglement. It would be interesting to extend the ideas in this paper to other spin-boson models, to open quantum systems that include a bosonic bath, and models with a periodic drive.

ACKNOWLEDGMENTS

We are thankful to Devendra Singh Bhakuni, Nilanjan Roy, Suhas Gangadharaiah, and Sebastian Wüster for fruitful comments and discussions. We are especially grateful to the anonymous referees for their extensive critical and constructive feedback that helped strengthen this paper. P.D. is grateful to IISERB for the Ph.D. fellowship. A.S. acknowledges financial support from SERB via Grant No. CRG/2019/003447, and from DST via the DST-INSPIRE Faculty Award (Grant No. DST/INSPIRE/04/2014/002461).

APPENDIX: THERMAL PHASE TRANSITION

We now show how the analytical expression for the transition temperature may be obtained. We begin with the expression for the partition function of the Dicke model written in the form of a double integral [Eq. (9)]:

$$Z(N,T) = \int \frac{d^2\alpha}{\pi} e^{-\beta|\alpha|^2} [\mathrm{Tr} e^{-\beta h}]^N = \int \frac{d^2\alpha}{\pi} e^{-\beta|\alpha|^2} \left(2\cosh\left\{\frac{\beta\epsilon}{2}\left[1+\frac{16\lambda^2\alpha^2}{\epsilon^2 N}\right]^{1/2}\right\}\right)^N. \tag{A1}$$

Here α is real, so $|\alpha| = |\alpha^*|$. Now

$$\int \frac{d^2\alpha}{\pi} = \int_0^\infty r dr \int_0^{2\pi} \frac{d\theta}{\pi} = 2\int_0^\infty r dr. \tag{A2}$$

Defining $y = \frac{r^2}{N}$ and

$$\phi(y) = -\beta y + \ln\left(2\cosh\left\{\frac{\beta\epsilon}{2}\left[1+\frac{16\lambda^2 y}{\epsilon^2}\right]^{1/2}\right\}\right), \tag{A3}$$

we have

$$Z(N,T) = N\int_0^\infty dy \exp[N\phi(y)]. \tag{A4}$$

Since we are interested in the thermodynamic limit where $N \to \infty$, we can invoke Laplace's method [86], and the integral is given by

$$Z(N,T) = N\frac{C}{\sqrt{N}} \max_{0\leqslant y\leqslant\infty} \exp\{N[\phi(y)]\} \tag{A5}$$

where C is some constant. To find the maximum of the function $\phi(y)$, we compute its derivative:

$$\phi' = -\beta + \frac{\beta 4\lambda^2}{\epsilon}\frac{1}{\eta}\tanh\left(\frac{\beta\epsilon\eta}{2}\right) \tag{A6}$$

where

$$\eta = \left[1+\frac{16\lambda^2 y}{\epsilon^2}\right]^{1/2}. \tag{A7}$$

Putting

$$\phi' = 0, \tag{A8}$$

we get

$$\eta = \frac{4\lambda^2}{\epsilon}\tanh\left(\frac{\beta\epsilon\eta}{2}\right). \tag{A9}$$

The hyperbolic tangent function is a monotonically increasing function and is bounded above by unity. Since $\eta \geqslant 1$ by definition [Eq. (A7)], if $4\lambda^2 < \epsilon$, there is no solution for Eq. (A9). On the other hand, for $4\lambda^2 > \epsilon$, the solution depends on the value of β. The critical value of the inverse temperature β_c can be computed by putting $\eta = 1$ and is given by

$$\beta_c = \frac{2}{\epsilon}\tanh^{-1}\left(\frac{\epsilon}{4\lambda^2}\right). \tag{A10}$$

Thus substituting $\epsilon = \frac{\omega_0}{\omega}$ and $\lambda = \frac{g}{\omega}$, we have an exact expression for the transition temperature:

$$T_c = \frac{1}{\beta_c} = \left(\frac{\omega_0}{2\omega}\right)\frac{1}{\tanh^{-1}\left(\frac{\omega\omega_0}{4g^2}\right)}. \tag{A11}$$

[1] S. Haroche, in *Conference on Coherence and Quantum Optics* (Optical Society of America, 2007), p. CTuF2.

[2] H. Kimble, Q. Turchette, N. P. Georgiades, C. Hood, W. Lange, H. Mabuchi, E. Polzik, and D. Vernooy, in *Coherence and Quantum Optics VII* (Springer, New York, 1996), pp. 203–210.

[3] M. Mirhosseini, E. Kim, X. Zhang, A. Sipahigil, P. B. Dieterle, A. J. Keller, A. Asenjo-Garcia, D. E. Chang, and O. Painter, Nature (London) **569**, 692 (2019).

[4] J. Vidal and S. Dusuel, Europhys. Lett. **74**, 817 (2006).

[5] S. Ashhab, Y. Matsuzaki, K. Kakuyanagi, S. Saito, F. Yoshihara, T. Fuse, and K. Semba, Phys. Rev. A **99**, 063822 (2019).

[6] U. Bhattacharya, S. Dasgupta, and A. Dutta, Phys. Rev. E **90**, 022920 (2014).

[7] S. Dasgupta, U. Bhattacharya, and A. Dutta, Phys. Rev. E **91**, 052129 (2015).

[8] K. Furuya, M. C. Nemes, and G. Q. Pellegrino, Phys. Rev. Lett. **80**, 5524 (1998).

[9] A. Lakshminarayan, Phys. Rev. E **64**, 036207 (2001).

[10] J. N. Bandyopadhyay and A. Lakshminarayan, Phys. Rev. Lett. **89**, 060402 (2002).

[11] J. N. Bandyopadhyay and A. Lakshminarayan, Phys. Rev. E **69**, 016201 (2004).

[12] A. Tanaka, H. Fujisaki, and T. Miyadera, Phys. Rev. E **66**, 045201(R) (2002).

[13] M. Žnidarič and T. Prosen, Phys. Rev. A **71**, 032103 (2005).

[14] P. Jacquod, Phys. Rev. Lett. **92**, 150403 (2004).

[15] S. Ghose and B. C. Sanders, Phys. Rev. A **70**, 062315 (2004).

[16] R. Demkowicz-Dobrzański and M. Kuś, Phys. Rev. E **70**, 066216 (2004).

[17] Y. S. Weinstein and C. S. Hellberg, Phys. Rev. Lett. **95**, 030501 (2005).

[18] A. Lakshminarayan and V. Subrahmanyam, Phys. Rev. A **67**, 052304 (2003).

[19] N. Lambert, C. Emary, and T. Brandes, Phys. Rev. Lett. **92**, 073602 (2004).

[20] C. Emary and T. Brandes, Phys. Rev. E **67**, 066203 (2003).

[21] C. Emary and T. Brandes, Phys. Rev. Lett. **90**, 044101 (2003).

[22] J. Vidal, S. Dusuel, and T. Barthel, J. Stat. Mech.: Theory Exp. (2007) P01015.

[23] R. Lewis-Swan, A. Safavi-Naini, J. J. Bollinger, and A. M. Rey, Nat. Commun. **10**, 1 (2019).

[24] K. Baumann, R. Mottl, F. Brennecke, and T. Esslinger, Phys. Rev. Lett. **107**, 140402 (2011).

[25] J. Klinder, H. Keßler, M. Wolke, L. Mathey, and A. Hemmerich, Proc. Natl. Acad. Sci. USA **112**, 3290 (2015).

[26] M. P. Baden, K. J. Arnold, A. L. Grimsmo, S. Parkins, and M. D. Barrett, Phys. Rev. Lett. **118**, 199901(E) (2017).

[27] P. Kirton, M. M. Roses, J. Keeling, and E. G. Dalla Torre, Adv. Quantum Technol. **2**, 1800043 (2019).

[28] R. H. Dicke, Phys. Rev. **93**, 99 (1954).

[29] E. Kadantseva, W. Chmielowski, and A. Shumovsky, in *Nonlinear Optics in Solids* (Springer, New York, 1990), pp. 37–41.

[30] P. Kirton and J. Keeling, New J. Phys. **20**, 015009 (2018).

[31] K. Hepp and E. H. Lieb, Ann. Phys. (NY) **76**, 360 (1973).

[32] Y. K. Wang and F. T. Hieo, Phys. Rev. A **7**, 831 (1973).

[33] P. Pérez-Fernández and A. Relaño, Phys. Rev. E **96**, 012121 (2017).

[34] G.-L. Zhu, X.-Y. Lü, S.-W. Bin, C. You, and Y. Wu, Front. Phys. **14**, 1 (2019).

[35] S. L. Sondhi, S. Girvin, J. Carini, and D. Shahar, Rev. Mod. Phys. **69**, 315 (1997).

[36] P. Cejnar, J. Jolie, and R. F. Casten, Rev. Mod. Phys. **82**, 2155 (2010).

[37] R. Casten and E. McCutchan, J. Phys. G **34**, R285 (2007).

[38] J. Ma and X. Wang, Phys. Rev. A **80**, 012318 (2009).

[39] A. Osterloh, L. Amico, G. Falci, and R. Fazio, Nature (London) **416**, 608 (2002).

[40] J. Reslen, L. Quiroga, and N. F. Johnson, Europhysics Letters **69**, 8 (2004).

[41] J. Chávez-Carlos, M. A. Bastarrachea-Magnani, S. Lerma-Hernández, and J. G. Hirsch, Phys. Rev. E **94**, 022209 (2016).

[42] E. Tsukerman, Phys. Rev. B **95**, 115121 (2017).

[43] M. A. Alcalde and B. Pimentel, Physica A **392**, 3765 (2013).

[44] M. Caprio, P. Cejnar, and F. Iachello, Ann. Phys. (NY) **323**, 1106 (2008).

[45] P. Stránský, M. Macek, and P. Cejnar, Ann. Phys. (NY) **345**, 73 (2014).

[46] P. Cejnar and P. Stránský, Phys. Rev. E **78**, 031130 (2008).

[47] J. E. García-Ramos, P. Pérez-Fernández, and J. M. Arias, Phys. Rev. C **95**, 054326 (2017).

[48] P. Cejnar, P. Stránský, M. Macek, and M. Kloc, J. Phys. A **54**, 133001 (2021).

[49] A. Pal and D. A. Huse, Phys. Rev. B **82**, 174411 (2010).

[50] R. Nandkishore and D. A. Huse, Annu. Rev. Condens. Matter Phys. **6**, 15 (2015).

[51] F. Alet and N. Laflorencie, C. R. Phys. **19**, 498 (2018).

[52] J. Karthik, A. Sharma, and A. Lakshminarayan, Phys. Rev. A **75**, 022304 (2007).

[53] P. Pérez-Fernández, A. Relaño, J. M. Arias, P. Cejnar, J. Dukelsky, and J. E. García-Ramos, Phys. Rev. E **83**, 046208 (2011).

[54] P. Pérez-Fernández, P. Cejnar, J. M. Arias, J. Dukelsky, J. E. García-Ramos, and A. Relaño, Phys. Rev. A **83**, 033802 (2011).

[55] W. Beugeling, A. Andreanov, and M. Haque, J. Stat. Mech.: Theory Exp. (2015) P02002.

[56] T. Brandes, Phys. Rev. E **88**, 032133 (2013).

[57] M. A. Bastarrachea-Magnani, S. Lerma-Hernández, and J. G. Hirsch, Phys. Rev. A **89**, 032101 (2014).

[58] M. A. Bastarrachea-Magnani, S. Lerma-Hernández, and J. G. Hirsch, Phys. Rev. A **89**, 032102 (2014).

[59] P. Stránský and P. Cejnar, Phys. Lett. A **380**, 2637 (2016).

[60] D. Poilblanc, T. Ziman, J. Bellissard, F. Mila, and G. Montambaux, Europhysics Letters **22**, 537 (1993).

[61] Y. Y. Atas, E. Bogomolny, O. Giraud, and G. Roux, Phys. Rev. Lett. **110**, 084101 (2013).

[62] M. A. Bastarrachea-Magnani, B. López-del Carpio, J. Chávez-Carlos, S. Lerma-Hernández, and J. G. Hirsch, Phys. Rev. E **93**, 022215 (2016).

[63] N. Macé, F. Alet, and N. Laflorencie, Phys. Rev. Lett. **123**, 180601 (2019).

[64] J. Lindinger, A. Buchleitner, and A. Rodríguez, Phys. Rev. Lett. **122**, 106603 (2019).

[65] A. J. Scott, Phys. Rev. A **69**, 052330 (2004).

[66] R. Radgohar and A. Montakhab, Phys. Rev. B **97**, 024434 (2018).

[67] U. T. Bhosale and M. S. Santhanam, Phys. Rev. E **95**, 012216 (2017).

[68] M. Kloc, P. Stránský, and P. Cejnar, Ann. Phys. (NY) **382**, 85 (2017).
[69] S. A. Hill and W. K. Wootters, Phys. Rev. Lett. **78**, 5022 (1997).
[70] W. K. Wootters, Phys. Rev. Lett. **80**, 2245 (1998).
[71] W. K. Wootters, Quantum Inf. Comput. **1**, 27 (2001).
[72] K. A. Dennison and W. K. Wootters, Phys. Rev. A **65**, 010301(R) (2001).
[73] V. Vedral, Phys. Rev. Lett. **90**, 050401 (2003).
[74] D. P. DiVincenzo, M. Horodecki, D. W. Leung, J. A. Smolin, and B. M. Terhal, Phys. Rev. Lett. **92**, 067902 (2004).
[75] G. Adesso and A. Datta, Phys. Rev. Lett. **105**, 030501 (2010).
[76] J. Maziero, H. C. Guzman, L. C. Céleri, M. S. Sarandy, and R. M. Serra, Phys. Rev. A **82**, 012106 (2010).
[77] J. Lindinger and A. Rodríguez, Phys. Rev. B **96**, 134202 (2017).
[78] M. Pino, V. E. Kravtsov, B. L. Altshuler, and L. B. Ioffe, Phys. Rev. B **96**, 214205 (2017).
[79] M. Serbyn, Z. Papić, and D. A. Abanin, Phys. Rev. B **96**, 104201 (2017).
[80] M. Kloc, P. Stránský, and P. Cejnar, Phys. Rev. A **98**, 013836 (2018).
[81] M. A. Bastarrachea-Magnani, S. Lerma-Hernández, and J. G. Hirsch, J. Stat. Mech.: Theory Exp. (2016) 093105.
[82] P. Cejnar and P. Stránský, Phys. Lett. A **381**, 984 (2017).
[83] M. V. Berry and M. Tabor, Proc. R. Soc. A **356**, 375 (1977).
[84] O. Bohigas, M. J. Giannoni, and C. Schmit, Phys. Rev. Lett. **52**, 1 (1984).
[85] W. Buijsman, V. Gritsev, and R. Sprik, Phys. Rev. Lett. **118**, 080601 (2017).
[86] H. Jeffreys, B. Jeffreys, and B. Swirles, *Methods of Mathematical Physics* (Cambridge University, New York, 1999).